Pergamon

Geochimica et Cosmochimica Acta, Vol. 68, No. 8, pp. 1889–1899, 2004

0016-7037/04 $30.00 + .00

doi:10.1016/j.gca.2003.10.031

A rocking multianvil: Elimination of chemical segregation in fluid-saturated high-pressure experiments

MAX W. SCHMIDT* and PETER ULMER

Institute for Mineralogy and Petrology, ETH Zentrum, CH 8092 Zurich, Switzerland

(*Received June* 26, 2003; *accepted in revised form October* 16, 2003)

Abstract—Fluid saturated high-pressure experiments often result in strongly zoned experimental charges, this hinders experimentation in chemically homogeneous systems which in turn has serious consequences on equilibration, reaction progress, and (apparent) phase stabilities. In order to overcome these problems, a 600-ton press accommodating either a multianvil or end-loaded piston cylinder module has been mounted in such a way that it can be turned by 180°, thus inverting its position in the gravity field. During turning, hydraulic pressure, heating power, and cooling water remain connected allowing fully controlled pressures and temperatures during experiments.

A series of experiments at 13 GPa, 950°C, on a serpentine bulk composition in the MgO-SiO_2-H_2O system demonstrates that continuous turning at a rate of 2 turns/min results in a nearly homogeneous charge composed of phase E + enstatite. The same experiment at static conditions resulted in four mineral zones: quench phase E, enstatite, enstatite + phase E, and phase E + phase A. Phase A disappears in experiments at a turning rate $\geq$1 turn/min. A static 15-min experiment shows that zonation already forms within this short time span. Placing two short capsules within a single static experiment reveals that the fluid migrates to the hot spot in each capsule and is not gravitationally driven toward the top. The zonation pattern follows isotherms within the capsule, and the degree of zonation increases with temperature gradient (measured as 10 °C within a capsule) and run time.

Our preferred interpretation is that Soret diffusion causes a density-stratified fluid within the capsule that does not convect in a static experiment and results in temperature dependant chemical zonation. The aggravation of zonation and appearance of additional phases with run time can be explained with a dissolution-reprecipitation process where the cold spot of the capsule is relatively MgO enriched and the hot spot relatively SiO_2 and H_2O enriched (at 13 GPa and 950°C). Rocking and tilting of a stratified fluid induces Rayleigh-Taylor instabilities, causing chemical rehomogenization. If turning is faster than the time required to build significant chemical potential gradients in the fluid, chemical zonation in the distribution of the solids is suppressed.

1. INTRODUCTION

Generally, solubilities of silicates and oxides in aqueous fluids increase with increasing pressure and temperature. Aqueous fluids in equilibrium with silicates at pressures of a few hundred MPa contain a few weight percent of dissolved material (e.g., 1.8 wt% SiO_2 at 0.2 GPa, 900°C in a pure H_2O-SiO_2 system; Manning, 1994), but 3 GPa is sufficient to increase solubilities to tens of percent (e.g., 22 wt% SiO_2 at 3 GPa, 900°C; Manning, 1994). A similar increase in cation solubility in hydrous fluids has been reported for the MgO-SiO_2-H_2O system where increasing pressure also results in an increase in the MgO/SiO_2 ratio of dissolved components in the fluid phase (Nakamura and Kushiro, 1974; Stalder et al., 2001; Mibe et al., 2002). This incongruent dissolution together with the high solubilities in aqueous fluids in high-pressure experiments cause significant problems in experimental systems designed to investigate hydrous phase stabilities. In fact, fractionation and the resulting chemical zonation is unavoidable in static fluid-saturated high-pressure experiments, at least as long as a perfectly homogeneous temperature distribution cannot be achieved.

It is common practice in chemically simple systems (e.g. MgO-SiO_2-H_2O, Al_2O_3-SiO_2-H_2O ± CaO) containing phases with constant compositions (e.g., clinohumite, talc, phase A, diaspore, topaz-OH, phase egg, lawsonite, zoisite) to extract the bulk of the run product mechanically from the capsule and to prepare smear slides for X-ray diffraction studies. Reaction progress and direction of reaction are monitored by relative peak intensities in X-ray diffractograms. However, the result obtained by this method can be seriously in error due to chemical segregation, which potentially allows a phase on the unstable side (e.g., talc) of a cross-reaction (e.g., talc + forsterite = enstatite + fluid) to increase in proportion despite representing part of the unstable assemblage at run conditions. Within a capsule, a zone of monomineralic talc (or talc ± enstatite) could be followed by a zone of enstatite and then a zone of forsterite (±enstatite) such that talc and forsterite abundances increase with respect to the starting material, although talc and forsterite are in separated zones within the capsule and do not coexist in the experiment. "Bulk extraction" studies thus suffer from the fact that information on chemical zonation, reaction textures, and potential disequilibrium is lost. Consequently, discrepancies among different studies are difficult to reconcile. Examples for large discrepancies in experimental data are common in the MgO-SiO_2-H_2O system and concern reactions involving the "hydrous alphabet phases"

* Author to whom correspondence should be addressed (max.schmidt@erdw.ethz.ch).

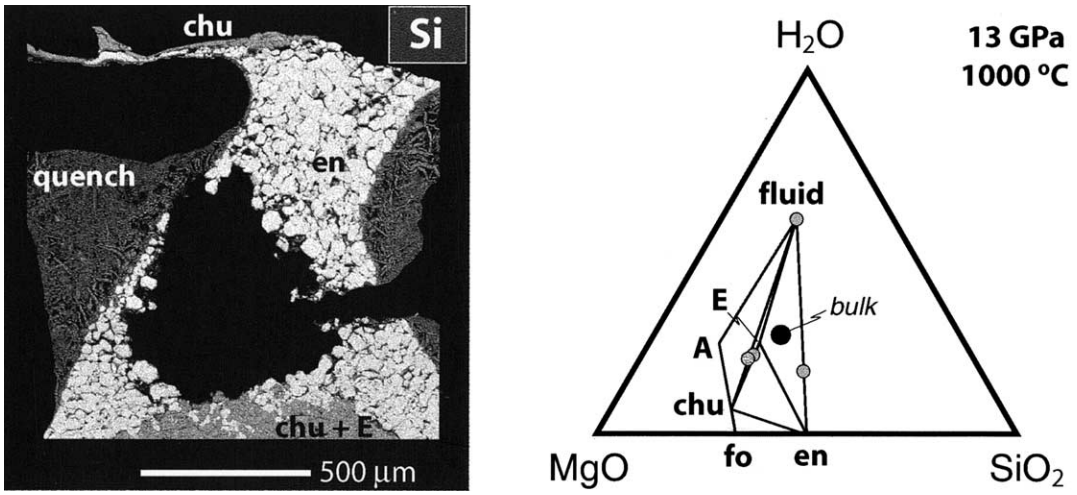

Fig. 1. (a) Si-Kα distribution map and zonations in an experiment from Stalder and Ulmer (2001) at 13 GPa, 1000°C; (b) Schematic representation of compositions of zones in the MgO-SiO_2-H_2O ternary.

(e.g., phase A, $Mg_7Si_2O_8(OH)_6$; phase E, approximately $Mg_{2.27}Si_{1.26}H_{2.4}O_6$), serpentine, talc ($Mg_3Si_4O_{10}(OH)_2$), clinohumite ($Mg_9Si_4O_{16}(OH)_2$), and chondrodite ($Mg_5Si_2O_8(OH)_2$). Most of the cross-reactions involving these phases that are relevant for natural peridotite compositions were studied in several laboratories (e.g., talc + forsterite = enstatite + H_2O: Kitahara et al., 1966; Yamamoto and Akimoto, 1977; Chernosky et al., 1985; Guggenheim, 1994; Ulmer and Trommsdorff, 1995; Wunder and Schreyer, 1997; Pawley, 1998; forsterite + H_2O = phase A + enstatite and the stability of phase E: Yamamoto and Akimoto, 1977; Khodyrev and Agoshkov, 1986; Kanzaki, 1991; Luth, 1995; Ohtani et al., 1995; Ulmer and Trommsdorff, 1995; Wunder, 1998; Bose and Navrotsky, 1998; Irifune et al., 1998; for a summary and discussion see Ulmer and Trommsdorff, 1999), but an agreement on the pressure-temperature range for particular phase assemblages is virtually absent. Major discrepancies predominantly concern cross-reactions, whereas reactions defining terminal stabilities of a given phase show a much better consistency. It is common to attribute such discrepancies to differences in the nature and composition of the starting material (which probably is correct in some cases). However, we argue that for cross-reactions, chemical segregation within the capsules is one of the main sources for disagreement and has hindered the building of a coherent database in the MSH system.

An example of chemical differentiation within an experimental charge from a static experiment from Stalder and Ulmer (2001) is presented in Figure 1a: An experiment on serpentine composition at 13.0 GPa, 1000 °C resulted in a capsule composed of four zones: (1) clinohumite + enstatite, (2) acicular phase E (quench from fluid phase), (3) enstatite, and (4) phase E + clinohumite + enstatite. Approximate bulk compositions of the zones are plotted in Figure 1b. This experiment contained a total of 11 wt% H_2O in the bulk with approximately 3 wt% bound in the hydrous phases. The remaining 8 wt% H_2O were apparently concentrated at the top and along the sides of the capsule; the latter exhibit a large amount of acicular quench phase E. It is exceedingly difficult to interpret reaction progress and stability relations from such an experiment where the bulk compositions of the individual observed zones traverse a series of compositional fields (Fig. 1b).

The pressures at which chemical zonation in fluid-saturated experiments becomes a serious experimental problem depend on the chemical system and on fluid-rock ratios. Our experience indicates that (i) in a CaO-Al_2O_3-SiO_2-H_2O-system problems did not occur to at least 8 GPa (Schmidt, 1995), (ii) in K-rich systems, chemical zonation in compositions with significant amounts of free fluid occurred at 1.5–2 GPa (Schmidt, 1996), and (iii) in a MgO-SiO_2-H_2O-system problems were obvious at 6 GPa and possibly occured at 3 GPa (Stalder and Ulmer, 2001).

This report presents a new type of apparatus, a “rocking” multianvil (named in analogy to rocking autoclaves) designed to overcome chemical segregation by forcing the fluid to migrate and to “stir” experimental systems in order to assist sluggish reactions.

2. THE ROCKING MULTIANVIL

A 600-ton O-frame press with a total weight of about 3.8 metric tons was suspended on a support frame (Fig. 2) through two half-axes fixed to the sides of the O-frame. The axes are near the centerline of gravity for O-frame + hydraulic ram + multianvil module. The multianvil module can be exchanged with a piston-cylinder module with the 600-ton hydraulic cylinder acting as the end-load ram. The weight distribution is then balanced within 5 kg (at 1 m radius) through additional weights fixed near the end of the O-frame. This is necessary in order to allow smooth automated rotation. Rotation is achieved through a 60-cm-diameter sprocket wheel directly mounted to the side of the O-frame and driven through a chain, transmission, and a small 24 V DC motor. The drive system was dimensioned such that one 180° turn is achieved in 29 s. The DC motor is controlled by a programmable logical unit, which allows adjustment of the resting interval between two turns. Automated inversion of the sample and thus the direction of the gravity vector acting on the sample is then achieved through cycles of a forward turn, a rest interval, a backward turn, and a rest

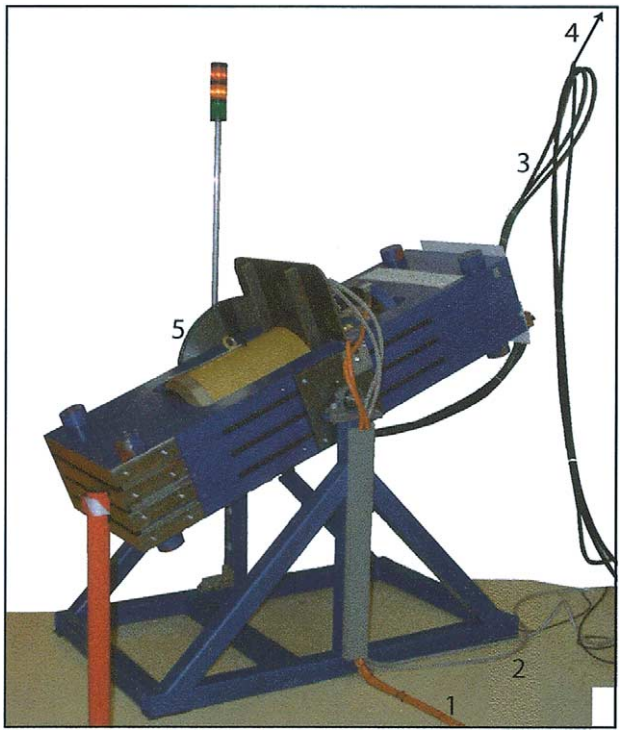

Fig. 2. Rocking multianvil device; 600-ton O-frame press with 6/8 cylindrical multianvil module. 1: Power cables; 2: cooling water hoses; 3: hydraulic pressure hoses; 4: pull-out wire; arrow indicates where fixed to the wall; 5: sprocket wheel.

interval. Hydraulic connections (max. 700 bar) are assured through 8-m-long flexible pressure hoses mounted with a "pull-out" wire to the nearby laboratory wall, such that the hoses are wrapped 180° around the press during the turning phase. Flexible power cables, cooling water hoses, and thermocouple compensation wires are loosely fixed near the axis. Although nothing could fall out of the press during rotation at pressure, the hydraulic cylinder is bolted to the press, and a drop in oil pressure below an adjustable value would bring the press to a stop in upright position. When turning, the immediate surroundings of the press are closed off; when idle, the press is secured to the frame by a large bolt.

3. EXPERIMENTAL AND ANALYTICAL DETAILS

The rocking multianvil is equipped with a cylindrically constrained Walker-type module (Walker et al., 1990). Tungsten carbide cubes of 32 mm edge length with 8-mm truncations (TEL) were employed in combination with 14-mm-edge-length prefabricated MgO-octahedra and pyrophyllite gaskets. The assembly consists of a zirconia sleeve, a stepped $LaCrO_3$ heater, a Mo disk and ring, MgO spacers inside the heater, and an axial $W_{95}Re_5$-$W_{74}Re_{26}$ thermocouple. All parts are fabricated in our machine shop and have tolerances of ±0.02 mm, assuring exactly reproducible conditions and especially thermal gradients in each experiment. Pressure was calibrated using coesite-stishovite (9.3 GPa, 1200°C; Yagi and Akimoto, 1976; Zhang et al., 1996) and forsterite-wadsleyite (14.5 GPa, 1400°C; Morishima et al., 1994) transitions.

The starting material was welded into 1.6 mm OD Au capsules that were pressed into a cylinder with ≤ 2.5 mm length, i.e., slightly shorter than the thickened central part of the furnace. Two experiments were run with two capsules in the central part of the furnace, each 1.3 mm long. In one of these two experiments, a second thermocouple was placed through the center of the furnace with the thermocouple junction situated between the two capsules and close to the MgO-insulation sleeve.

The starting material was composed of a mixture of brucite and talc corresponding to serpentine composition ($Mg_3Si_2O_5(OH)_4$) and is identical to the one used by Stalder and Ulmer (2001). During the experiments, it turned out that all experiments contained small amounts of magnesite. At the time of the experiments, we attributed the appearance of magnesite to CO_2-absorption from air and formation of a small amount of hydromagnesite in the starting material (sitting for several years in a desiccator), although in the starting material, we could not detect hydromagnesite or magnesite by X-ray diffraction. Repeated drying at 220°C in a vacuum furnace did not result in magnesite-free run products. The amount of CO_2 necessary to form magnesite is minuscule at our run conditions (950°C, 13 GPa); calculations show that an X_{CO_2} of $2.6 \cdot 10^{-4}$ in the fluid is sufficient to saturate a forsterite+ enstatite+ fluid[1] assemblage with magnesite. This would translate into 0.08 μg CO_2 or 0.02 μg carbon in the capsule. As a matter of fact, the CO_2 present in the run product was not necessarily absorbed from the air; a second possibility is that during welding of the capsules, a small amount of graphite deposited from the graphite electrode of the arc welder into the capsule, leading to magnesite in the run products. In a present experimental series on hydrous alphabet phases, we replaced the graphite electrode by a silver electrode, and in the few subsequent experiments, we did not observe any magnesite.

Run products were imaged with a secondary electron microscope, and phase compositions were analyzed with a Cameca SX50 electron microprobe. The identity of the phases was additionally verified by micro-Raman spectroscopy.

The preparation of the experimental run products for analysis posed significant difficulties due to poor grain coherence resulting from the fluid-saturated subsolidus conditions. All capsules where multiply impregnated with low viscosity epoxy and polished, but despite careful and slow polishing, some of the experimental charges display areas where the solid material broke out. These "holes" are not indicative for fluid-filled cavities as fluid-filled areas characteristically show abundant quench precipitate (needles of phase E). To obtain meaningful cross sections through experimental capsules, care was taken that polished sections are oriented in a plane that includes the axis of the cylindrical capsule.

4. RESULTS

A static experiment from Stalder and Ulmer (2001) at 13.8 GPa, 950°C was repeated six times at 13 GPa, 950°C (Table 1). NZ01 was turned every 15 min starting 15 min after the beginning of heating; turning was ended in the initial position 15 min before quench. NZ03 and NZ04 were turned at a frequency of 1 turn/min and 1 turn/30 s (i.e., continuously); turning started before heating and ended after quench. NZ05 was run statically for 15 min. NZ06 and NZ07 had two capsules and were run statically, NZ06 with the axial thermocouple toward the top and NZ07 with the axial thermocouple toward the bottom.

4.1. Turning Frequency Series

Enstatite + phase E + fluid represents the stable assemblage at the selected experimental condition of 13.0 GPa and 950°C in a chemically homogeneous system on serpentine composition (experiment NZ04, Table 1). This result is in accordance with the interpretation of Stalder and Ulmer (2001). However, the static experiment of Stalder and Ulmer yielded a capsule

[1] Reliable data of phase E are not available, but a similar X_{CO_2} is expected for phase E+ enstatite+ fluid.

Table 1. Run table.[a]

Experiment	P (GPa)	T (°C)	t (h)	Turning frequency	Resulting zones
MSH47[b]	13.8	950	25	Static	quench/en/en+E/E+A
NZ01	13.5	950	4	15 min	en/en+E/en+E+mgs/E+A+mgs
NZ03	13.5	950	4	1 min	en/en+E/en+E+mgs
NZ04	13.5	950	4	30 s	en+E/en+E+mgs
NZ05	13.5	950	0.25	Static	en/en+E/en+E+mgs
NZ06	13.5	950	4	Static	u.cap.: quench/en/en+E/E/E+mgs/A+E+mgs l.cap.: quench/en/en+E/E+mgs
NZ07	13.5	950	4	Static	u.cap.: quench/en/en+E/E+mgs l.cap.: quench/en/E/E+mgs/A+E+mgs

[a] Abbreviations: A, phase A; E, phase E; en, clinoenstatite; mgs, magnesite; quench, fluid quench (mainly acicular phase E); u.cap., upper capsule; l.cap, lower capsule.
[b] Experiment performed by Stalder and Ulmer (2001).

consisting of four zones separated by sharp boundaries (Fig. 3a). The top zone consisted of a loose intergrowth of needles of phase E, which was interpreted as quench from fluid residing in a pocket at the top end of the capsule. The second zone consisted of enstatite, the third one of short prismatic phase E plus some enstatite, and the bottom zone of phase E + phase A. Phase proportions within the zones were estimated by Stalder and Ulmer (2001) and resulting bulk compositions plotted in Figure 3b. In this experiment, the uppermost zone composed of solid phases has the highest SiO_2/MgO ratio and the bottom zone the lowest one. The lowest zone contains a phase (phase A) that is not stable in the bulk composition of the starting material at the specific run conditions. Quench from the fluid phase is only found in the uppermost part of the capsule.

Experiment NZ01 (Table 1), turned every 15 min (Figs. 3c, d), yielded a capsule with much less zoning; in particular the sharp boundaries between individual zones disappeared. Nevertheless, an enstatite-only zone is observed in the side portions of the capsule. Along most of its boundary, the enstatite-only zone gradually developed into an enstatite + phase E zone. The amount of phase E increases until enstatite disappears near one end of the capsule, where phase A occurs in a relatively thin zone (<120 μm; note that a physically meaningful top end cannot be defined anymore, but that this end of the capsule is opposite to the axial thermocouple). At the same end of the capsule, some texturally equilibrated magnesite crystallized, due to a small amount of CO_2 in the starting material. Although enstatite and magnesite are in proximity, there is no direct contact between these two phases, suggesting that they do not coexist with each other (Figs. 4a, b). Compared with the static experiment, the chemical gradient within the capsule is significantly reduced; however, zoning and appearance of additional phases are not completely eliminated.

Experiment NZ03, turned every minute, yielded a charge (Figs. 3e, f) consisting exclusively of enstatite, phase E, and magnesite. Phase A did not form at this turning frequency. Along the sides of the capsule an enstatite-only zone developed, phase E becomes gradually more abundant away from this zone and toward one end of the capsule enstatite amounts to less than 5 vol%. Magnesite crystallized at the phase E–rich end of the capsule, which is again the end of the capsule opposite to the axial thermocouple.

In experiment NZ04, turned every 30 s (i.e., continuously; Figs. 3g, h), $>90\%$ of the capsule volume is occupied by a homogeneous phase E + enstatite mix with an equilibrated texture (Fig. 4c). There is no apparent gradient in the relative proportions of phase E and enstatite apart from a small zone consisting almost entirely of enstatite along the sides of the capsule and in a second zone located at the end opposite to the axial thermocouple where magnesite crystallized and enstatite contents are slightly decreased.

In summary, increasing the turning frequency leads to an almost homogeneous capsule composed of enstatite + phase E. Phase A disappears between turning frequencies of 4 and 60 turns/h. The enstatite only and, thus, SiO_2-rich zone is always located along the side of the capsule. The relative volume of the enstatite-only zone diminishes with increasing turning frequency. One end of the capsule always contains some magnesite due to minor CO_2 or carbon present in the starting material. The same capsule end is the portion of the capsule where phase A can occur and where phase E reaches its highest and enstatite its lowest modal abundance. Thus, the highest MgO concentrations are observed at the capsule end opposite to the thermocouple. A zone with obvious quench precipitate from the fluid was absent in the "rocking" experiments. It appears that rocking leads to a more or less homogeneous distribution of fluid in the intergranular space.

4.2. Timescale of Segregation

The results of the series of experiments with variable turning frequency suggest that zonations are formed through a relatively rapid process (acting within minutes). In order to test this working hypothesis, a short static experiment (NZ05) with a 15-min run time was performed.

The experiment (Fig. 5a) reveals that strong zonation is already present after this short time span: An enstatite-only zone developed along the sides of the capsule, followed by a zone that exhibits a gradual increase in the relative proportion of phase E until enstatite becomes a minor constituent. In the center and at both ends of the capsule, minor magnesite crystallized with predominantly phase E. In this 15-min experiment, phase A is absent. The zoning pattern resembles the hourglass-shaped distribution of isotherms that are often observed in high-pressure multianvil experiments, i.e., resembles the temperature distribution within the capsule, assuming that the hot spot was located centrally at the side and the cold spots at the ends of the capsule (e.g., Walter et al., 1995). In this

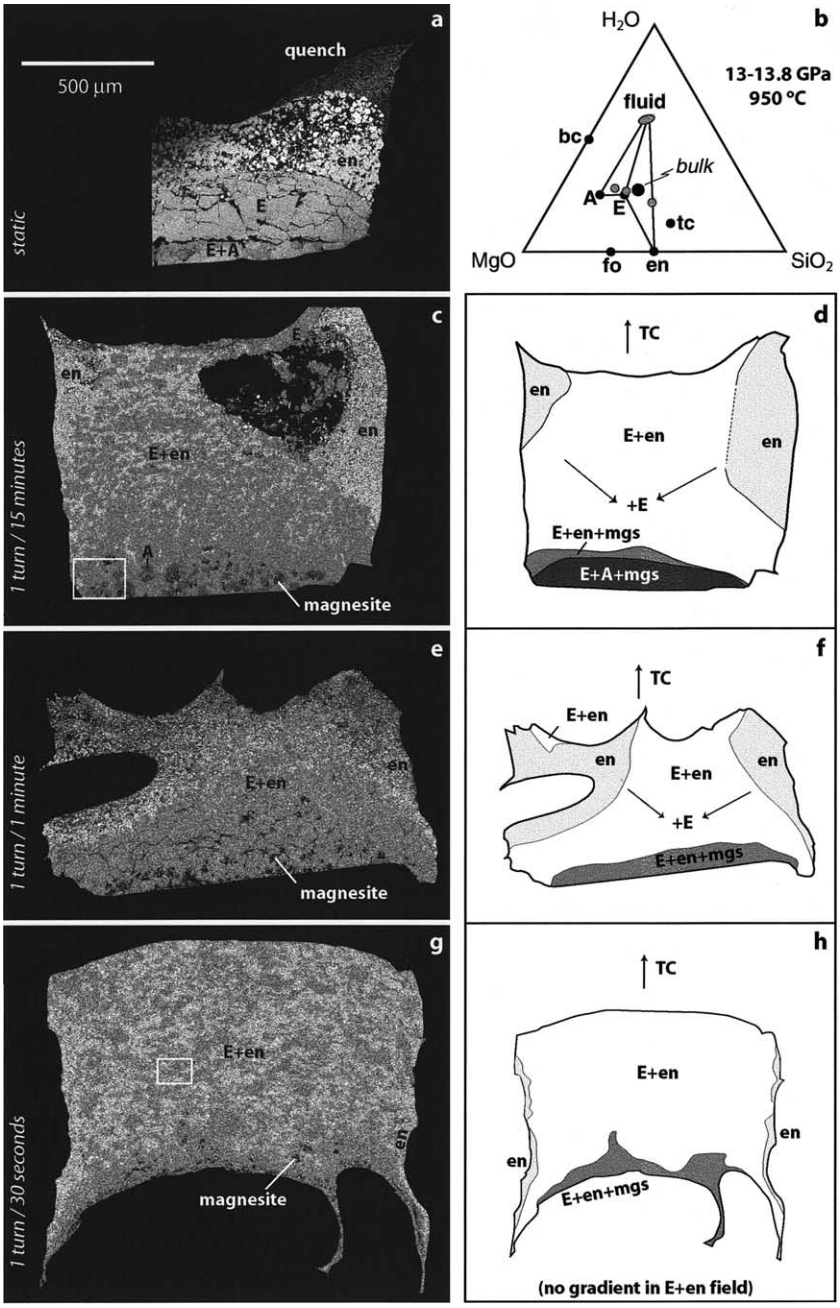

Fig. 3. Results from a series of experiments with variable turning frequency. Si-Kα distribution maps of experimental charges and sketches of the zoning patterns. (a) Static experiment at 13.8 GPa, 950°C (from Stalder and Ulmer, 2001); the capsule is strongly zoned with quench-precipitate residing at the top, followed by enstatite, phase E_+ enstatite, and phase E_+ phase A zones. (b) Starting material compounds (brucite, bc, and talc, tc), bulk composition of the starting material (equivalent to serpentine) and approximate compositions of zones observed in the static experiment of (a). (c–h) experiments at 13 GPa, 950°C, with different turning frequencies. The arrows labeled TC in the sketches indicate in which direction the axial thermocouple was situated. (c, d) One turn/15 mins, experiment NZ01, Table 1. (e, f) One turn/1 min NZ03. (g, h) One turn/30 ss (continuous turning, NZ04). White frames correspond to images in Figures 4a–c.

experiment, quench-precipitate from the fluid is situated along the sides, i.e., in the hot spot of the capsule, and not at the upper end of the capsule. The 15-min static experiment implies that phase A does not form immediately at the beginning (=heating) of the experiment, but through a time-dependant process during longer duration experiments.

4.3. Spatial Distribution of Zones and the Role of Gravity

The previous experiment suggests that the spatial distribution of zones, i.e., their geometrical pattern, is not simply related to gravity but rather to the temperature distribution within the capsule. In order to understand the zoning geometry

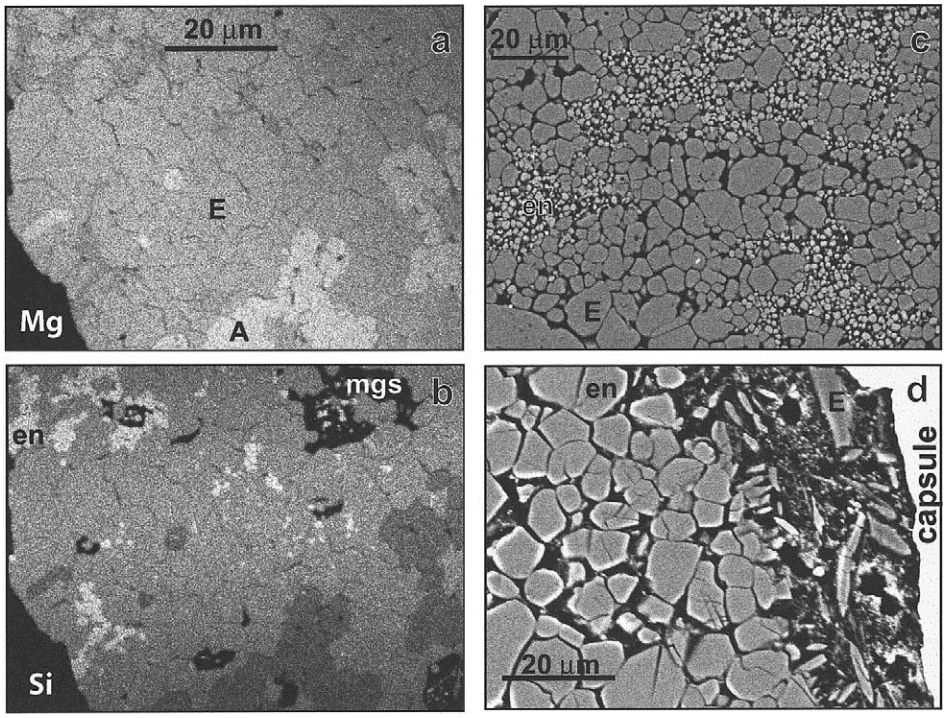

Fig. 4. (a) Si-Kα and (b) Mg-Kα distribution maps at the MgO-rich end of experiment NZ01 (1 turn/15 min, Figs. 3c,d): Magnesite (mgs), enstatite (en), phase E (E) and phase A (A). (c) BSE image of equilibrated texture of phase E + enstatite in the continuously rocked experiment NZ04 (Figs 3g, h). (d) BSE image of quench precipitate (phase E) from fluid phase residing at the side of the upper capsule of experiment NZ07 (see black frame in Fig. 7).

and thus the driving forces of chemical zoning, two static experiments of 4 h run duration were performed, each containing two identical capsules within the central thickened portion of the $LaCrO_3$ furnace. Experiment NZ06 (Fig. 6) was designed such that in both capsules the gravity vector is in the same direction relative to the capsules orientation, but the temperature gradient is opposite in the two capsules. In the upper capsule, temperature increases downward (same general direction as gravity); in the lower capsule, temperature increases upward (opposite to gravity). This concept assumed that the hot spot in our assembly is located exactly in the middle of the furnace. However, zoning in experiment NZ06 is not symmetrical to a plane situated between the two capsules but symmetrical to a plane through the center of the capsule adjacent to the thermocouple (the lower capsule in Fig. 6). The symmetrically zoned lower capsule of experiment NZ06, has a central enstatite-only zone, followed by phase E + enstatite, and phase E + enstatite + magnesite zones toward both ends of the capsule. Quench precipitate is observed along the sides of the capsule. Zoning in the upper capsule of experiment NZ06 is asymmet-

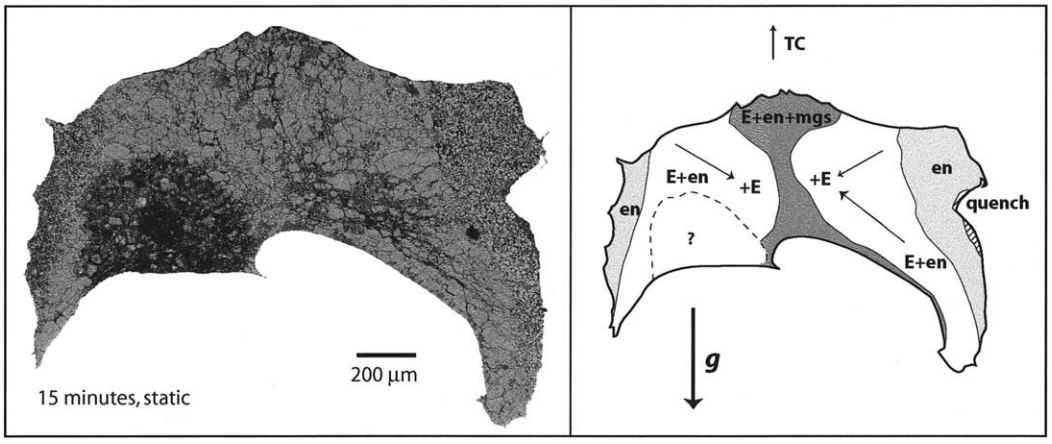

Fig. 5. Fifteen-minute duration static experiment NZ05. BSE image showing lateral zoning and sketch diagram depicting phase distributions within the charge, zones follow isotherms within the capsule. Note the absence of phase A.

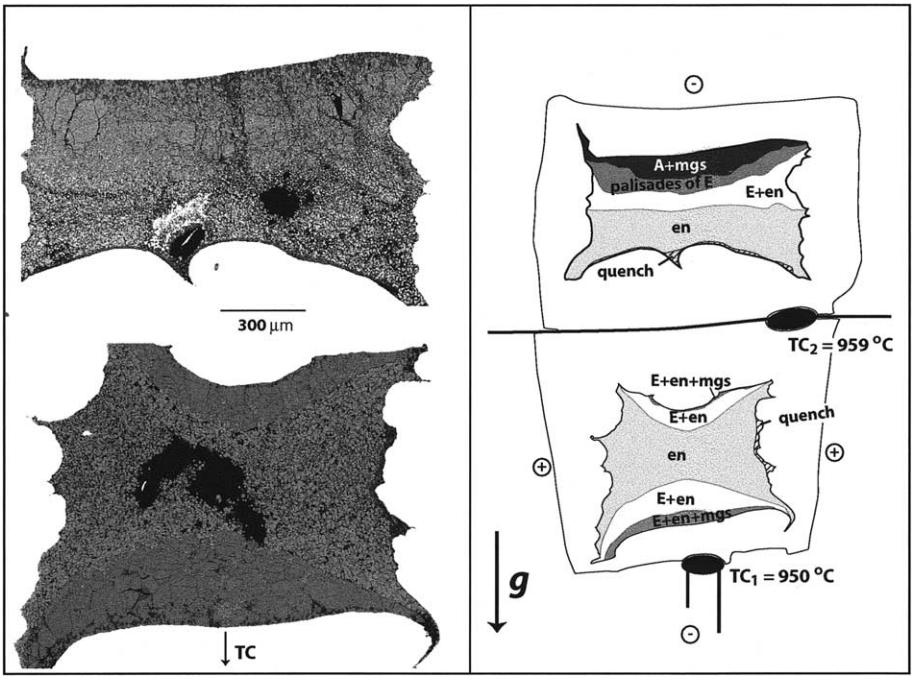

Fig. 6. Two-capsule experiment with axial thermocouple located at the bottom (NZ06). The capsule adjacent to the thermocouple is symmetrically zoned; the upper capsule reveals asymmetrical zoning and has quench precipitate from the fluid concentrated in a zone at the bottom of the capsule, indicating that fluid migration is not gravity driven. The symmetry of zonations can be explained by a temperature gradient driven process, provided that the hot spot was situated at the side of the capsule adjacent to the thermocouple (as indicated by plus signs = hot spot, and minus signs = cold spots). In this case fluid concentrates in the hot spot of the capsule. SiO_2-rich zones form near the hot spot, MgO-rich zones near the cold spot.

rical. Quench precipitate is located at the *lower* end of the capsule, followed by an enstatite-only zone, a phase E + enstatite zone, a phase E-only zone, and a phase A + magnesite zone toward the top of the capsule (Fig. 6).

In order to verify that the observed asymmetry is due to an asymmetric arrangement of assembly components,[2] and not caused by gravity, a second two-capsule experiment (NZ07) was performed with the octahedron turned upside down with respect to the previous experiment. In other words, the geometrical arrangement within the octahedron was identical, but NZ07 had the axial thermocouple upward instead of downward as in NZ06 (Fig. 7).

In experiment NZ07, a zoning pattern similar to the previous experiment (NZ06) is observed: the capsule adjacent to the thermocouple (upper capsule in Fig. 7) is symmetrically zoned with a central enstatite-only zone followed by a phase E + enstatite, phase E-only, and a phase E + magnesite zone. These zones are geometrically less symmetrical than in the homologous capsule in NZ06, probably due to the very thick and unevenly welded side of this capsule; the large mass of Au influences the thermal gradient. Similar to experiment NZ06, the capsule away from the thermocouple is asymmetrically zoned. The sequence of zones is comparable and is constituted from top to bottom by: quench precipitate—enstatite only—phase E only—phase E + magnesite—phase A + phase E + magnesite. The individual zones in this capsule have remarkably sharp boundaries, comparable to the zone boundaries observed in the static experiment shown in Figure 3a. In NZ07, quench precipitate is situated again along the side of the capsule adjacent to the axial thermocouple, whereas the other capsule has quench precipitate at the end directed toward the axial thermocouple. In summary, both experiments show the same geometry of zoning with reference to the thermocouple and asymmetric arrangement of assembly components, i.e., with respect to the thermal gradient. In contrast, sample orientation relative to the gravity field does not have any apparent consequence on the observed zoning.

5. SEGREGATION DRIVEN BY THERMAL GRADIENTS

In experiment NZ06, the upper capsule had fluid concentrated at the lower end (Fig. 6), and the lower capsule had fluid concentrated along its sides. This observation demonstrates that formation of fluid pockets, and fluid migration within a capsule is not simply a gravity-driven process; if due to gravity, fluid should buoyantly migrate upward, because fluid is the least dense phase in the capsule. A consistent explanation of the observed zonation is obtained if fluid migration and chemical zonation are dominantly temperature-gradient driven processes. In this case, the zoning implies that the hot spot in our experiments is systematically shifted by about 500 μm away from

[2] Although the $LaCrO_3$ furnace itself is strictly symmetric, one end of the furnace is filled by a MgO-sleeve, a thermocouple ceramics made of corundum, and by thermocouple wire, the other end by a simple MgO-cylinder.

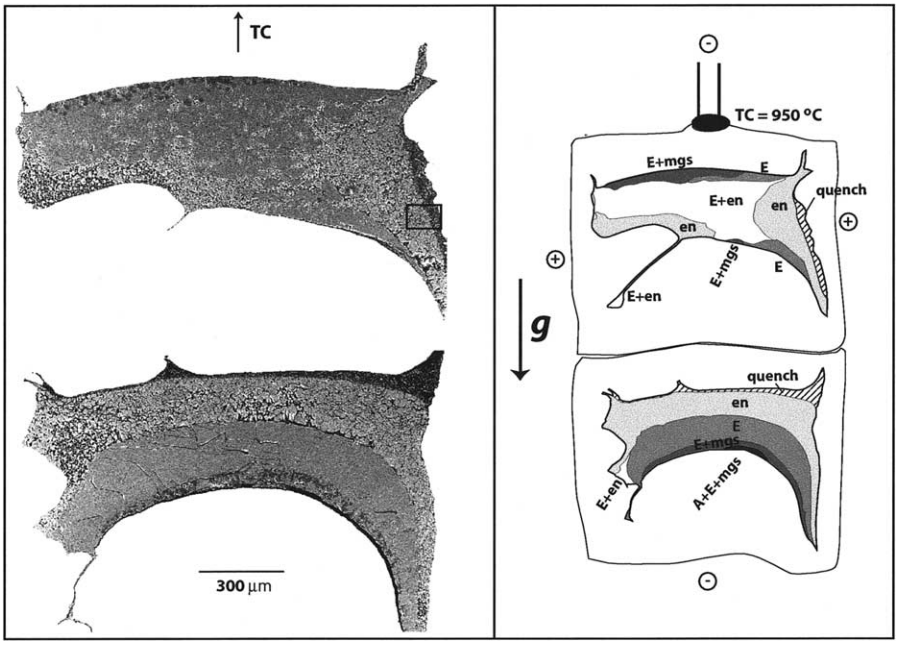

Fig. 7. Two-capsule experiment with axial thermocouple located at the top (NZ07), i.e., relative to NZ06 (Fig. 6), the octahedron has been mounted upside down. In accordance with experiment NZ06, the capsule adjacent to the thermocouple is symmetrically zoned, and the other capsule shows asymmetrical zoning. In other words, the zonation pattern relative to the position of the axial thermocouple is identical as in NZ06, but relative to gravity is turned by 180°. The plus signs indicate the position of the hot spot, the minus signs the positions of the relative cold spots. The black frame locates the image of Figure 4d.

the geometrical center of the furnace toward the axial thermocouple (as indicated by the plus and minus signs in Figs. 6 and 7).

Based on the hypothesis obtained from the "two capsule experiments," fluid migrates towards the hot spot, i.e., to the center side of the capsule adjacent to the axial thermocouple, and in the other capsule to the end directed toward the thermocouple, respectively. The SiO_2-concentration gradient resulting from the solid phase parageneses reveals a similar pattern: relatively SiO_2-rich zones (i.e., enstatite only) form near the hot spot, whereas MgO-rich zones (phase E only, and phase A–containing zones) are formed near the cold spots of each individual capsule. Magnesite always precipitates at the coldest end of a capsule, which is most distant from the enstatite-only zones. The geometrical pattern and the inferred compositions of the solid phase zones in all our experiments can be reconciled by fluid-migration accompanied by increasing $\mu SiO_2/\mu MgO$ toward the hot spot. It should, however, be noted that absolute concentrations of Si or Mg dissolved in the fluid and absolute values of chemical potentials (i.e., μSiO_2 and μMgO) have not been determined in this study. The present experiments only constrain the relative variation of the ratio of the chemical potentials, $\mu SiO_2/\mu MgO$, within the capsule. Therefore, the following discussion and Figure 8 are based on this ratio.

6. A MODEL FOR CHEMICAL SEGREGATION

The experimental observations are coherently interpretable if chemical segregation is purely temperature driven, and the geometrical zoning pattern is directly related to the temperature variation within the capsule (Fig. 8). Soret diffusion, which causes a steady-state chemical gradient within a (previously homogeneous) liquid exposed to a temperature gradient (Chipman, 1926; Bierlein, 1954; Snowdon and Turner, 1960; Cygan and Carrigan, 1992), plays a central role in this model.

(1) Soret diffusion causes a chemical gradient in the fluid whereby $\mu SiO_2/\mu MgO$ increases toward the hot spot of the capsule (at our experimental condition), causing enstatite to precipitate and phase E to be dissolved in the hot zone. Concomitantly, the high-entropy fluid phase migrates to and concentrates at the hot spot. At the cold end of the capsule, enstatite is dissolved and phase E is preferentially precipitated, leading to an enrichment in MgO.

(2) When 100% of the starting material recrystallizes into equilibrium phases, Soret diffusion is fast enough to cause a strong gradient and thus zonation within less than 15 min. The time for our experimental system to approach Soret steady state is given as

$$t_{ss} = \frac{4 \cdot \lambda^2}{\pi^2 \cdot D} \quad (1)$$

(Carrigan and Cygan, 1986), where λ is the inner capsule length of $1.2\ 10^{-3}$ m and D the chemical diffusivity. The latter was experimentally determined to be $1.6\ 10^{-7}\ m^2 s^{-1}$ for SiO_2 in aqueous solution at 950°C, 1 GPa (Watson and Wark, 1997) which results into $t_{ss} = 4$ s. Compared to our study, the diffusivity measurements were obtained at relatively low pressures, fluid densities, and concentrations (approximately 1 molal), and thus, the above diffusivity

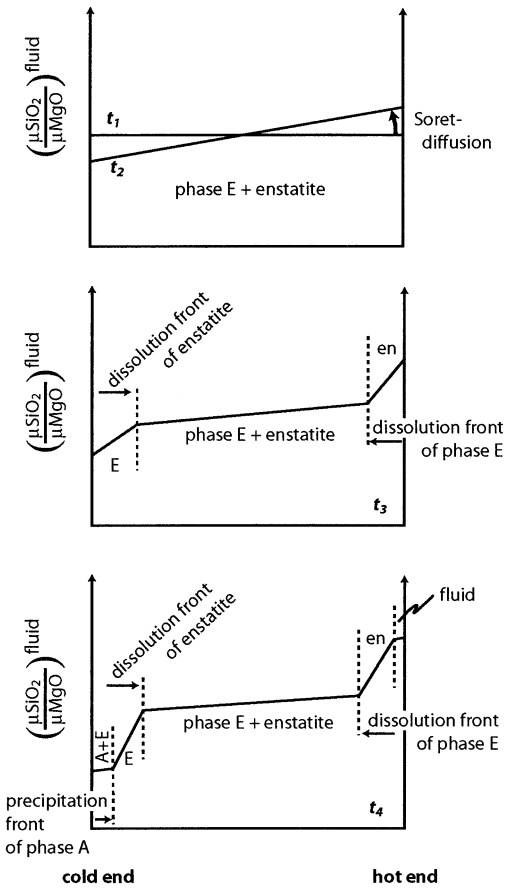

Fig. 8. Schematic diagram illustrating the evolution of $\mu SiO_2/\mu MgO^{fluid}$ over time in a high-pressure experiment. In the very beginning, a Soret diffusion gradient develops in a capsule containing phase E + enstatite. As a consequence of the Soret gradient, enstatite dissolves at the cold end and phase E at the hot end. When one phase is completely dissolved, the composition of the fluid phase (in equilibrium with a single solid phase) is no longer buffered, and concentration gradients may considerably steepen. As a consequence, an additional phase may precipitate (phase A), again resulting in a buffered fluid composition. Note that the present study can neither constrain the concentration gradients nor a single chemical potential gradient; the only thermodynamic property defined is the relative variation in the $\mu SiO_2/\mu MgO^{fluid}$ ratio.

represents probably an upper limit. Effective diffusivities in concentrated solutions at high pressures might be 1–2 orders of magnitude lower, yielding time spans that are proportionally longer. From experimental measurements and thermodynamic modeling of brines at much lower pressures and temperatures, Cygan and Carrigan (1992) concluded that half an hour is sufficient to establish a Soret steady-state concentration profile over 2 mm with a thermal gradient of 1°C/mm. It is thus very likely, that Soret diffusion establishes a significant concentration gradient over the present experimental timescale.

(3) Provided that the chemical composition gradient resulting from Soret diffusion within the fluid remains undisturbed, a dissolution-precipitation process aggravates the zonation in the distribution of solid phases. Over time, this process leads to complete dissolution of the MgO-rich phase(s) at the hot end (i.e., phase E) and the SiO_2-rich phase(s) at the cold end (i.e., enstatite) of each capsule. Once a "single solid phase zone" (e.g., phase E only) has formed, the fluid composition is no longer buffered, it may strongly change its composition, and saturation in additional phases may be reached. This process is observed at the cold end of the capsule, where the fluid becomes saturated in phase A, which then precipitates, again buffering the fluid composition.

(4) In most cases, Soret diffusion increases, the absolute concentrations towards the cold spot (e.g., Caldwell and Eide, 1981). This is consistent with our experimental observation that zoning is stronger and solid-phase zone boundaries considerably sharper in cases where the cold zone is directed downward in the capsule. In this case, the solute-rich denser fluid resides gravitationally stable at the bottom of the capsule, and the less dense fluid containing less solute resides toward the top of the capsule.

(5) Experiment NZ06, performed with two thermocouples, has shown that the temperature gradient within our central thickened furnace does not exceed 10°C significantly. However, such a small thermal gradient is obviously sufficient to cause the observed zoning.

7. MAINTAINING HOMOGENEITY THROUGH TURNING

Continuous rocking results in continuous inversion of the sample in the gravity field that acts on the experimental system and produces an almost homogeneous charge, i.e., the strong chemical segregation observed in static fluid-saturated high-pressure experiments can be suppressed. As argued above, the zonation is not gravity driven. However, zonation can be avoided by inverting the sample position in the gravity field acting on the experimental system. This apparent contradiction is reconciled by the following model.

(1) Rocking or turning of the multianvil causes rehomogenization in the fluid phase. This cannot occur by stirring the fluid through its moment of inertia as the rocking movement is gentle and slow (turning occurs at an angular velocity of 60 s/360°, the capsule is situated at a radius of about 140 mm relative to the rotation axis of the apparatus). We thus suggest that Soret diffusion results in a density stratification that is stable without tilting the experimental system, but that tilting the system triggers Rayleigh-Taylor instabilities in a fluid in which density increases towards the top. To evaluate this scenario, the Rayleigh number can be calculated from

$$Ra = \frac{\alpha \cdot \rho \cdot k \cdot g \cdot \nabla T \cdot \lambda^2}{\mu \cdot \kappa_T}, \qquad (2)$$

where α is the thermal expansivity of the fluid, for pure H_2O this is $3.3 \cdot 10^{-5}°C^{-1}$, ρ is the density of the fluid (for pure H_2O, this is $1.79 \cdot 10^3$ kg $\cdot$ m^{-3} [both calculated at 13 GPa and 950°C from Halbach and Chatterjee, 1982, EoS]), k is the permeability estimated from porosity φ through $k \cong 10^{-7} \cdot \varphi^3$, φ is estimated from the amount of free fluid phase (8 wt%) to be 12 vol%. This value represents an upper limit assuming that the fluid phase will be equally distributed within the capsule. ∇T is the thermal gradient

measured to be $1 \cdot 10^4$°C $\cdot$ m^{-1} over the capsule length, λ is the inner capsule length of 1.2 10^{-3} m, κ_T is the thermal diffusivity, extrapolated to $6.6 \cdot 10^{-7}$ m^{2}s^{-1} at 950°C (Abramson et al., 2001), and μ is the viscosity of the fluid. This last parameter is the least certain one, as high pressure/temperature measurements do not exist. Nevertheless, the viscosity of our solute-rich fluid is estimated to be somewhere between pure supercritical H_2O (i.e., $1 \cdot 10^{-4}$ to $2 \cdot 10^{-4}$ Pa $\cdot$ s, Dudziak and Franck, 1966) and the least viscous hydrous silicate melt (i.e., wet basalt, 10^0 Pa $\cdot$ s).

Rayleigh-Taylor instabilities in porous materials may occur if the critical Rayleigh number of $4*\pi^2$ is exceeded (Turcotte and Schubert, 1982, p. 404). Eqn. 2 only considers density differences caused by thermal expansion of the fluid, and employing the viscosity of supercritical H_2O as a lower limit, Ra falls in the range 0.002–0.07. Higher viscosities, as might be appropriate for higher density, solute-rich fluids at high pressures, would further decrease the Rayleigh number. A density gradient in the fluid caused by thermal expansivity over a temperature gradient of 10°C is small compared to a density gradient caused by possible concentration gradients in the order of wt%. In order to assess this latter effect, we evaluated a concentration gradient of 1 wt% solute (which would be caused by Soret diffusion) by replacing $\alpha \cdot \nabla T$ in equation (2) by the appropriate density contrast. This increases the Rayleigh number to about 0.8. From these estimates, it appears to be highly unlikely that Rayleigh-Taylor instabilities would occur in a *horizontally* stratified fluid under our experimental conditions, confirming the experimental observations in static experiments.

(2) The observed ability of the fluid to collect in a particular zone of the capsule during subsolidus high-pressure experiments indicates that dihedral angles between fluids and silicates are generally less than 60° and that the fluid forms an interconnected network. Watson et al. (1990) and Mibe et al. (1999) argued that dihedral angles tend to decrease with increasing pressure and temperature thus increasing the interconnectivity, permeability, and mobility of the fluid. In an interconnected fluid, it is thus plausible that Soret diffusion occurs over the scale of the entire capsule and is not limited to individual isolated pores. Soret diffusion then causes chemical zonation in the static capsules.

(3) The critical Rayleigh number of $4*\pi^2$ applies to horizontal density stratifications. However, tilting should trigger Rayleigh-Taylor instabilities and thus mix the fluid effectively. This will reset the $\mu SiO_2/\mu MgO$-gradient in the fluid, but cannot result in an opposite gradient. Thus, once zonation has formed, rocking cannot eliminate this zonation as long as the solid phases form part of the stable assemblage within the given bulk composition.

(4) It follows that gravity has no direct role in the formation and persistence of chemical zonations in fluid-saturated high-pressure experiments, and that zonation patterns directly reflect the thermal field. Within a capsule, zonation is symmetrical to the rotation axis and has a subhorizontal "mirror plane" in cases where the hot spot is situated at the side of the capsule (the mirror plane indicating the position of the hot spot). Zonations are asymmetric when the hot spot is located toward one end or beyond the end of a capsule. It appears that zonation increases with increasing temperature gradients. However, very limited and experimentally unavoidable temperature gradients of $\leq$10°C/mm are already sufficient to cause substantial chemical segregation in static experiments.

8. CONCLUSIONS AND PERSPECTIVES

In this report, we describe a recipe to obtain chemically unzoned capsules from fluid-saturated high-pressure experiments. The optimal experiment has a hot spot exactly centered on the capsule. If complete recrystallization of the starting material occurs at the beginning of the experiment, it is necessary to rock the capsule before heating of the experiment with a frequency that is scaled to the capsule dimension and the Soret diffusion coefficient. In our example, 2 turns/min were barely sufficient. After the starting material has fully crystallized into equilibrium phases, lower turning frequencies are sufficient to maintain whatever was achieved in the initial heating period of the experiment. Once a compositional gradient has developed in the solid phases, it is too late; such a gradient cannot be reset by gravitationally driven convection of the fluid.

The rocking multianvil device causes movement of the fluid within the capsule and thus should promote reaction rates when compared to static systems. As a consequence, fluid-rock ratios could be lowered in low temperature experiments, thereby decreasing the chemical segregation problem even further. Generally, long run times are believed to result in "better" phase equilibria data. However, chemical segregation progressing with time through dissolution-reprecipitation processes produces an undesired effect. The rocking multianvil allows longer run times at relatively low (and hopefully constant) levels of chemical segregation. This provides the possibility to perform true equilibrium experiments in fluid-saturated high pressure systems. Further, experimental time series will monitor reaction progress rather than the added effects of chemical segregation and reaction progress.

The synthesis of monomineralic charges of hydrous alphabet phases at fluid excess conditions generally fails due to the chemical segregation within the charge. Yields of the desired phase often do not exceed 60%. The new rocking multianvil allows synthesis of near monomineralic run products through minimization of fluid-rock ratios and rehomogenization induced by rocking, thus providing monomineralic synthesis products for X-ray powder diffraction.

Acknowledgments—We thank J. A. D. Connolly for his his help explaining fluid dynamics equations, and John Holloway and two anonymous reviewers for their encouraging reviews.

Associate editor: B. Mysen

REFERENCES

Abramson E. H., Brown J. M., and Slutsky L. J. (2001) The thermal diffusivity of water at high pressures and temperatures. *J. Chem. Phys.* **115,** 10461–10463.

Bierlein J. A. (1954) A phenomenological theory of the Soret diffusion. *J. Chem. Phys.* **23,** 10–14.

Bose K. and Navrotsky A. (1998) Thermochemistry and phase equilibria of hydrous phases in the system MgO-SiO_2-H_2O: Implications

for volatile transport to the mantle. *J. Geophys. Res.* **103,** 9713–9719.

Caldwell D. R. and Eide S. A. (1981) Soret coefficient and isothermal diffusivity of acqueous solutions of five principal salt constituents of seawater. *Deep-Sea Research* **28A,** 1605–1618.

Carrigan C. R. and Cygan R. T. (1986) Implications of magma chamber dynamics for Soret-related fractionation. *J. Geophys. Res.* **91,** 11451–11461.

Chernosky J. V. J., Day H. W., and Caruso L. J. (1985) Equilibria in the system MgO-SiO_2-H_2O: Experimental determination of the stability of Mg-anthophyllite. *Am. Mineral.* **70,** 223–236.

Chipman J. (1926) The Soret effect. *J. Am. Chem. Soc.* **48,** 2577–2589.

Cygan R. T. and Carrigan C. R. (1992) Time-dependent Soret transport—Applications to brine and magma. *Chem. Geol.* **95,** 201–212.

Dudziak K. H. and Franck E. U. (1966) Messungen der Viskosität des Wassers bis 560 °C und 3500 bar. *Ber. Bunsenges. Phys. Chem.* **70,** 1120–1128.

Guggenheim E. (1994) Stabilitaet von Talk, Forsterit und Enstatit im Feld und im Experiment. Diploma, ETH.

Halbach H. and Chatterjee N. D. (1982) An emperical Redlich-Kwong-type equation of state for water to 1000 °C and 200 kbar. *Contrib. Mineral. Petrol.* **79,** 337–345.

Irifune T., Kubo N., Isshiki M., and Yamasaki Y. (1998) Phase transformations in serpentine and transportation of water into the lower mantle. *Geophys. Res. Lett.* **25,** 203–206.

Kanzaki M. (1991) Stability of hydrous magnesium silicates in the mantle transition zone. *Phys. Earth Planet. Int.* **66,** 307–312.

Khodyrev O. Y. and Agoshkov V. M. (1986) Phase transitions in serpentine in the MgO-SiO_2-H_2O system at 40–80 kbar. *Geochem. Int.* **23,** 47–52.

Kitahara S., Takenouchi S., and Kennedy G. C. (1966) Phase relations in the system MgO-SiO_2-H_2O at high temperatures and pressures. *Am. J. Sci.* **264,** 223–233.

Luth R. W. (1995) Is phase A relevant to the Earth's mantle? *Geochim. Cosmochim. Acta* **59,** 679–682.

Manning C. E. (1994) The solubility of quartz in H_2O in the lower crust and upper mantle. *Geochim. Cosmochim. Acta* **58,** 4831–4839.

Mibe K., Fujii T., and Yasuda A. (1999) Control of the location of the volcanic front by aqueous fluid connectivity in the mantle wedge. *Nature* **401,** 259–262.

Mibe K., Fujii T., and Yasuda A. (2002) Composition of aqueous fluid coexisting with mantle minerals at high pressure and its bearing on the differentiation of the Earth's mantle. *Geochim. Cosmochim. Acta* **66,** 2273–2285.

Morishima H., Kato T., Suto M., Ohtani E., Urakawa S., Utsumi W., Shimomura O., and Kikegawa T. (1994) The phase boundary between α- and β-Mg_2SiO_4 determined by in situ X-ray observation. *Science* **265,** 1202–12 –3.

Nakamura Y. and Kushiro I. (1974) Composition of the gas phase in Mg_2SiO_4-SiO_2-H_2O at 15 kbar. *Carnegie Inst. Washi. Year Book.* **73,** 255–258.

Ohtani E., Shibata T., Kubo T., and Kato T. (1995) Stability of hydrous phases in the transition zone and the upper most part of the lower mantle. *Geophys. Res. Lett.* **22,** 2553–2556.

Pawley A. R. (1998) The reaction talc + forsterite = enstatite + H_2O: New experimental results and petrological implications. *Am. Mineral.* **83,** 51–57.

Schmidt M. W. (1995) Lawsonite: Upper pressure stability and formation of of higher density hydrous phases. *Am. Mineral.* **80,** 1286–1292.

Schmidt M. W. (1996) Experimental constraints on recycling of potassium from subdcuted oceanic crust. *Science* **272,** 1927–1930.

Snowdon P. N. and Turner J. C. R. (1960) The Soret effect in some 0.01 normal aqueous electrolytes. *Trans. Faraday Soc.* **56,** 1409–1418.

Stalder R. and Ulmer P. (2001) Phase relations of a serpentine composition between 5 and 14 GPa—Significance of clinohumite and phase E as watet carriers into the transition zone. *Contrib. Mineral. Petrol.* **140,** 670–679.

Stalder R., Ulmer P., Thompson A. B., and Günther D. (2001) High pressure fluids in the system MgO-SiO_2-H_2O at upper mantle conditions. *Contrib. Mineral. Petrol.* **140,** 607–618.

Turcotte D. L. and Schubert G. (1982) *Geodynamics: Application of Continuum Physics to Geological Problems.* Wiley.

Ulmer P. and Trommsdorff V. (1995) Serpentine stability to mantle depths and subduction-related magmatism. *Science* **268,** 858–861.

Ulmer P. and Trommsdorff V. (1999) Phase relations of hydrous mantle subducting to 300 km. In *Mantle Petrology: Field Observations and High Pressure Experiments,* Vol. 6 (eds. Y. Fei, C. M. Bertka and B. O. Mysen), pp. 259-281. Geochemical Society, Special Publication.

Walker D., Carpenter M. A., and Hitch C. M. (1990) Some simplification to multianvil devices for high pressure experiments. *Am. Mineral.* **75,** 1010–1028.

Walter M., Thibault Y., Wei K., and Luth R. W. (1995) Characterizing pressure and temperature conditions in multi-anvil apparatus. *Can. J. Phys.* **73,** 273–286.

Watson E. B., Brenan J. M. and Baker D. R. (1990) Distribution of fluids in the continental mantle. In *Continental Mantle* (ed. M. A. Menzies), pp. 111-125. Clarendon Press.

Watson E. B. and Wark D. A. (1997) Diffusion of dissolved SiO_2 in H_2O at 1 GPa, with implications for mass transport in the crust and upper mantle. *Contrib. Mineral. Petrol.* **130,** 66–80.

Wunder B. (1998) Equilibrium experiments in the system MgO-SiO_2-H_2O (MSH): Stability of clinohumite-OH [$Mg_9Si_4O_{16}(OH)_2$], chondrodite-OH [$Mg_5Si_2O_8(OH)_2$] and phase A [$Mg_7Si_2O_8(OH)_6$]. *Contrib. Mineral. Petrol.* **132,** 111–120.

Wunder B. and Schreyer W. (1997) Antigorite: High-pressure stability in the system MgO-SiO_2-H_2O (MSH). *Lithos* **41,** 213–227.

Yagi T. and Akimoto S.-I. (1976) Direct determination of coesite-stishovite transition by in-situ X-ray measurements. *Tectonophysics* **35,** 259–270.

Yamamoto K. and Akimoto S.-I. (1977) The system MgO-SiO_2-H_2O at high pressures and temperatures—Stability field for hydroxyl-chondrodite, hydroxyl-clinohumite and 10 Å-phase. *Am. J. Sci.* **277,** 288–312.

Zhang J., Utsumi W., and Liebermann R. C. (1996) In situ X-ray observations of the coesite-stishovite transition: Reversed phase boundary and kinetics. *Phys. Chem. Mineral.* **23,** 1–10.